Asymmetric Hydrogen-Bonding of the Quinone Cofactor in Photosystem I Probed by ^{13}C-Labeled Naphthoquinones†

Yulia N. Pushkar, John H. Golbeck,‡ and Dietmar Stehlik*

Institut für Experimentalphysik, Freie Universität Berlin, Arnimallee 14, D-14195 Berlin, Germany

Herbert Zimmermann

Max-Planck Institut für Medizinische Forschung, Jahnstrasse 29, D-69120 Heidelberg, Germany

Received: July 26, 2003; In Final Form: October 27, 2003

In photosystem I (PS I) the phylloquinone secondary acceptor functions as a one electron gate similar to the Q_A quinone secondary acceptor in type II reaction centers. The quinone radical anion formed during charge separation as part of the $P_{700}^{+\bullet}$ $A_1^{-\bullet}$ radical pair state is known to have a highly asymmetric electron spin density distribution, which is attributed to asymmetric hydrogen bonding with the protein environment. Here, the native phylloquinone is replaced by specifically ^{13}C-labeled 2-methyl-1,4-naphthoquinones (2-methyl-4-^{13}C-1,4-naphthoquinone and 2-^{13}C-methyl-1,4-naphthoquinone) to probe the spin density distribution in two relevant quinone ring positions. The *men*B phylloquinone biosynthetic pathway mutant was used because it allows for efficient in vitro quinone replacement in isolated PS I trimers. X- and Q-band time-resolved EPR spectroscopy was used to determine the ^{13}C hyperfine tensors in the functional $P_{700}^{+\bullet}$ $A_1^{-\bullet}$ state. For 2-methyl-4-^{13}C-1,4-naphthoquinone anion radical the largest hyperfine tensor component $A_{zz} = 44$ MHz was found to be considerably larger than those determined in bacterial reaction centers. The PS I structure at 2.5 Å resolution shows a single H-bond from the backbone NH group of a specific leucine residue. Such a highly asymmetric H-bonding is confirmed here for the functional $P_{700}^{+\bullet}$ $A_1^{-\bullet}$state. Experimental evidence for an unusual backbone H-bond strength is analyzed by comparing the quinone binding site with that in bacterial reaction centers and possible mechanisms of increased H-bond strength are considered.

Introduction

In all photosynthetic organisms, the conversion of sunlight into chemical energy occurs in membrane-bound complexes referred to as photosynthetic reaction centers (RCs). In oxygenic photosynthesis, two extended RC complexes, photosystem I (PS I) and photosystem II (PS II), function in tandem. With the elucidation of the PS I structure at 2.5 Å resolution,[1,2] structural details have become available for the first time for a type I RC. However, to a large extent the functional significance of many of these features remains unclear. This is particularly evident when corresponding cofactor binding sites are compared between type I (PS I) and type II (purple bacteria, pb) RCs. Both share a common C_2 symmetric structural motif of transmembrane α-helices within a heterodimeric (in some type I RCs a homodimeric) protein complex. Thus, a common overall binding frame exists for the respective two branches of cofactors. In the course of photoinduced charge separation an electron is transferred from the primary electron donor P located near one side of the membrane to the first quinone acceptor Q on the other side of the membrane. In both types of RCs the first quinone acceptor functions as a one electron gate but to different sets of terminal acceptors. Despite the common overall structural framework, the detailed properties of the cofactors and their protein environment exhibit a considerable degree of variability, the functional significance of which remains largely unexploited. Various quinones native to other photosynthetic RCs have been shown to function in PS I, e.g., menaquinone of pbRC and even plastoquinone-9,[3,4] recruited from PS II when the biosynthesis of phylloquinone is blocked. Comparative EPR studies of type I (PS I) and type II (pb) RCs, see, e.g., refs 5 and 6, have shown that the orientation and observable protein cofactor interactions of the respective quinones differ. The recent PS I structure[1,2] has confirmed these partial results and extended substantially the detailed knowledge of the quinone binding sites. Thus, as shown in Figure 1, a detailed comparison of the quinone binding sites is now possible for the two types of RCs. As a complementary technique, spectroscopy can supply additional details of specific protein−cofactor interactions. For instance, in both types of RCs the quinones have a methyl group and an unsaturated hydrophobic side chain as ring substituents at adjacent ring positions between the two C═O groups. Magnetic resonance methods can yield hyperfine couplings of the protons in these two groups. They in turn can be correlated to asymmetric H-bonding between the quinone cofactor and the protein environment; see ref 7 for a review. Very different H-bonding schemes have been proposed between the two types of RCs as based on mutually supportive results by both spectroscopy and structure analysis as detailed in this work for PS I. Moreover, other substantial differences have been identified in the properties of the two types of RCs, e.g., redox potentials, electron transfer kinetics, and also magnetic tensor properties. Nevertheless, a key question remains largely unanswered: How do the differences in protein−cofactor interactions

† Part of the special issue "Jack H. Freed Festschrift".

* Corresponding author. Telephone: ×49-30-83855069. Fax: ×49-30-83856081. E-mail: Stehlik@physik.fu-berlin.de.

‡ On leave from: Department of Biochemistry and Molecular Biology, The Pennsylvania State University, University Park, PA 16802.

10.1021/jp0361879 CCC: $27.50
Published on Web 03/26/2004

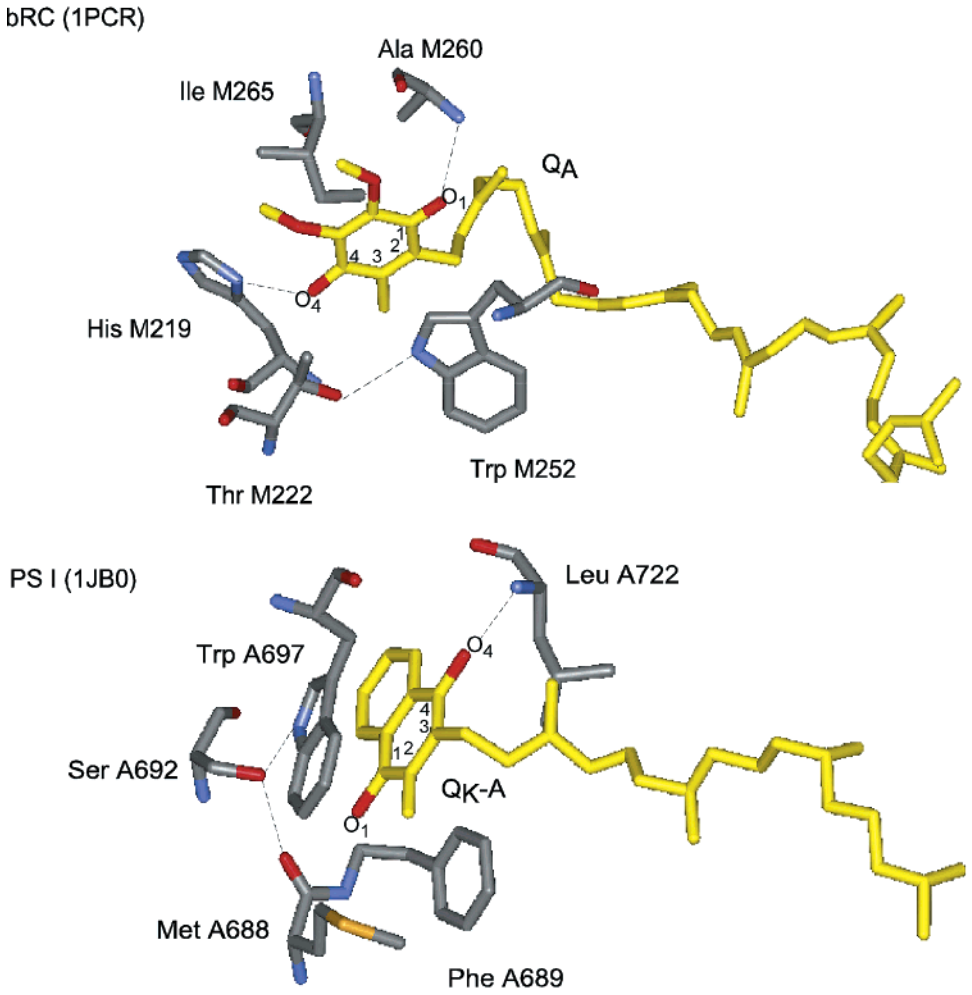

Figure 1. Comparison of the quinone binding sites Q_K-A in PS I and Q_A in bRC. Top: Binding pocket of Q_A in the M subunit of reaction centers from *R. sphaeroides* (PDB entry 1PCR, *Rb. Sphaeroides)*. Hydrogen bonds between the quinone carbonyl oxygens and M260 (peptide NH) and M219 (His-$N_\delta H$) are shown as dotted lines. Bottom: Structural model of the Q_K-A binding site in PS I as adapted from ref 1 (PDB entry 1JB0, *S. elongatus*). Residues are shown explicitly for those amino acids that are involved in identified protein−quinone interactions (π-stacking and H-bonding). The residues Trp (π-stacking) and Ser (part of an H-bond network involving the π-stacking Trp and the backbone of the Met ligand to A_0) were subjected to site directed mutagenesis.[13]

relate to and possibly control the quite different functional properties of the quinone acceptor in the two types of RCs?

In this situation, additional experimental information is of prime importance. Two strategies can be exploited: systematic modification of either the cofactor (by substitution) or its protein environment (by mutation). For example, we have studied PS I complexes with different artificial quinones in place of the native phylloquinone: 2-methyl-1,4-naphthoquinone differs from native phylloquinone by the absence of the phytyl side chain. Nevertheless, it can be incorporated successfully into the A_1 site, in phylloquinone biosynthetic pathway (*menB* or *menA*) mutants[8] or after organic solvent extraction of phylloquinone.[9] Moreover, time-resolved EPR (TR-EPR) techniques show that the artificial quinone in the functional charge separated state $P_{700}^{+\bullet}$ $A_1^{-\bullet}$ occupies a position and orientation identical to native phylloquinone. The functional competence of a monosubstituted 1,4-naphthoquinone makes it feasible to determine hyperfine tensors and spin densities in additional ring positions by the use of selectively isotopic labeled 2-methyl-1,4-naphthoquinones in PS I.

A similar strategy has been introduced and exploited previously to study the influence of asymmetric H-bonding on the π-spin density distribution in the ring of the reduced quinone acceptor of purple bacterial RCs. Extensive work by two magnetic resonance groups has been summarized.[7,10] A simple valence bond model (see, e.g., Figure 14 of ref 7) is adapted here as Figure 2 for the A_1 site in PS I. It correlates asymmetric H-bonding to the two carbonyl groups with the observed asymmetric and alternating π-spin density distribution over the quinone ring. An increased spin density is predicted for the ring carbon of the carbonyl group to which the dominating H-bond is attached. In accordance with the various possible resonance structures, the spin density is also increased at the ring carbons in meta-position to this C═O and at the oxygen of the other C═O group (with the weaker H-bond). A decreased spin density is predicted for all ring positions in between. Thus, an asymmetric and alternating spin density distribution is rationalized. Both the asymmetric spin density distribution and the underlying elementary valence bond model have been nicely confirmed for all relevant ring positions of the quinone acceptor in bRC; for a review see refs 7 and 10.

In the case of the reduced phylloquinone in PS I, a large proton hyperfine coupling has been measured for the CH_3 substituent position.[11,12] The deviation from the symmetric H-bonding found for the quinone in solution is at least twice as large as in the corresponding ring position of Q_A in the bRC and has been taken as indication of a correspondingly more asymmetric H-bonding situation in PS I than in the bRC in

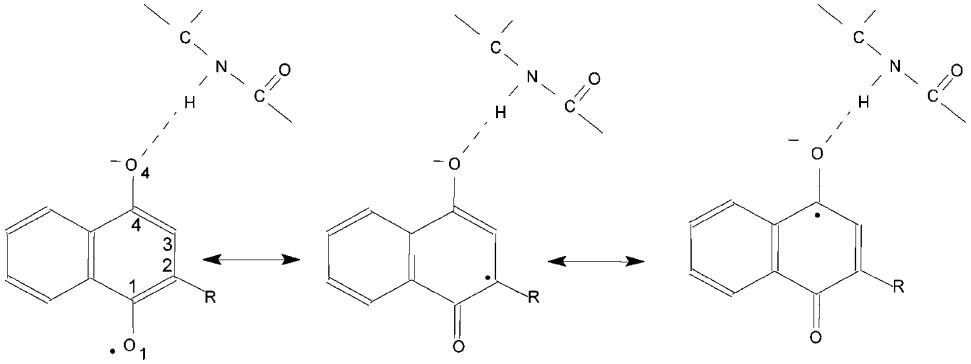

Figure 2. Valence bond model used to explain the spin density distribution of a 2-methyl-1,4-naphthoquinone anion radical hydrogen bounded to the backbone nitrogen. Note that for a hydrogen bond oxygen atom the electrostatic interaction of the partial positive charge at the proton increases the charge density at hydrogen bounded oxygen and decreases it in the ring and at oxygen without hydrogen bond. Concomitantly, the spin density is increased at position marked with the • (dot).

accordance with a single backbone H-bond suggested by the X-ray structure; see Figure 1, bottom. Moreover, the occurrence of a single H-bond corresponding to an unusually high spin density at the ring position ortho to the H-bonded quinone C═O group turned out to be remarkably stable for a series of modifications of either the specific 1,4-NQ substituents or point mutations in the Q_K-A environment.[13] To confirm the significance of this single H-bond as a structural element it is important to evaluate the spin density distribution in other relevant ring positions. According to Figure 2, the most significant ring position is the carbon atom of the H-bonding carbonyl group. Here, we report results for a ^{13}C isotope label in this carbonyl group, i.e. the C_4 position of the artificial 2-methyl-1,4-naphthoquinone in the functional A_1 site of PS I.

Material and Methods

Synthesis of ^{13}C-Labeled 2-Methyl-1,4-naphthoquinones. The synthesis of 2-methyl-4-^{13}C-1,4-naphthoquinone proceeds according to Scheme 1. The starting compound 2-methylcinnamic acid (**I**), prepared according to ref 14 by a modified Perkin reaction from benzaldehyde and propionic anhydride, was reduced to 2-methylcinnamyl alcohol (**II**) with $LiAlH_4$ in ether. Catalytic hydrogenation to 2-benzyl-1-propanol (**III**) was accomplished with fresh reduced Adam's catalyst PtO_2 in methanol. Conversion to the 2-benzylpropyl bromide (**IV**) with $SOCl_2$ was followed by carboxylation of the corresponding Grignard reagent with $^{13}CO_2$ (from $Ba^{13}CO_3$, −30 °C, ether) to 3-benzylbutyric acid-1-^{13}C (**V**). Cyclization to 2-methyl-4-^{13}C-4-tetralone (**VI**) was made via the acid chloride of **V** ($SOCl_2$, room temperature) with polyphosphoric acid as described for tetralone.[15] Clemmensen reduction of (**VI**) resulted in 2-methyl-4-^{13}C-tetraline (**VII**), followed by dehydrogenation with palladium on charcoal to 2-methyl-4-^{13}C-naphthalene (**VIII**). Oxidation with CrO_3 in the usual way yielded 2-methyl-4-^{13}C-1,4-naphthoquinone (**IX**).

For synthesis of 2-^{13}C-methyl-1,4-naphthoquinone the 2-naphthoic acid−carboxyl-^{13}C was prepared by carboxylation with $^{13}CO_2$ of 2-naphthylmagnesium bromide. The naphthoic acid was reduced by $LiAlH_4$ to 2-naphthalenemethanol-^{13}C followed by conversion to the bromide. Dehalogenation with $LiAlH_4$ resulted in 2-^{13}C-methylnaphthalene. Oxidation with CrO_3 yielded the 2-^{13}C-methyl-1,4-naphthoquinone.

The precise labeling of the 2-methyl-1,4-naphthoquinones and the percentage of isotope as well as the chemical purity were checked by ^{13}C and ^1H NMR and mass-spectrometry and found to be better than 99%.

SCHEME 1: Synthesis of 2-Methyl-4-^{13}C-1,4-naphthoquinone.

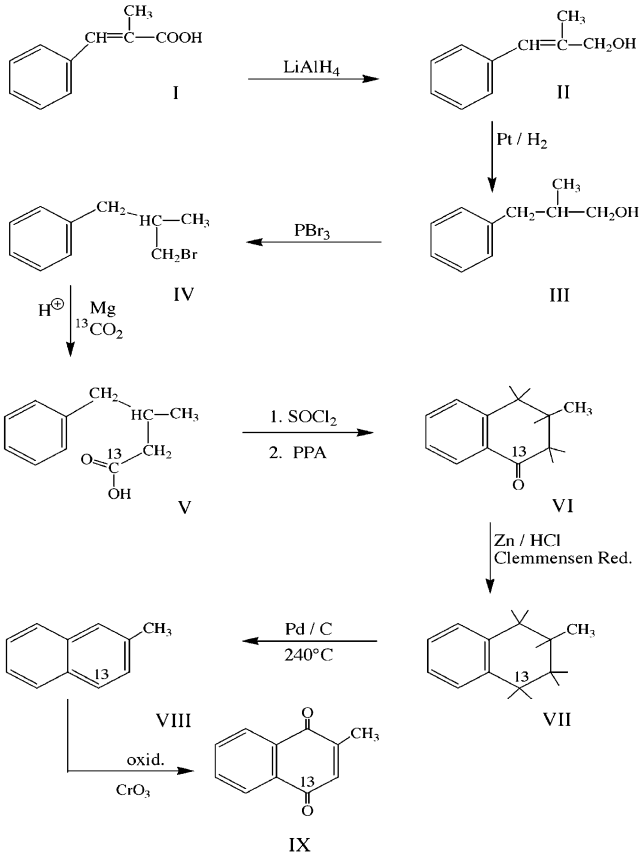

Preparation of Photosystem I with ^{13}C-Labeled Quinones. A 100-fold molar excess of quinone (10 μL of 0.034 M solution of quinone in ethanol) was added to PS I trimers (150 μL in Tris buffer pH 8.3 containing 0.2% Triton X-100) isolated from *menB* mutant cells of *Synechocystis sp*. PCC 6803. Incubation was carried out at room temperature (2−4 h) with intensive stirring. The PS I particles were washed 2 times with 150 μL buffer solution to remove excess quinone; the final volume of sample was 150 μL.

The former method has a distinct advantage over the organic solvent extraction method because PS I complexes remain unaffected during the quinone exchange. The carotenoids and chlorophylls are preserved in their native state while they are removed to a large extent during the solvent extraction method. In general, in vitro quinone replacement in PS I complexes from the *menB* mutant will leave the PS I complexes intact.

TABLE 1: ^{1}H Hyperfine Tensor Principal Values (MHz) of Residues in the $-CH_3$ Position of Different Quinones in Type I (PS I) and Type II (bRC) Reaction Centers and Spin Densities at the Corresponding Carbon Atom Position in the Quinone Ring, to Which the Respective Substituent Is Attached

	type I RC Q_K in PS I reaction center				type II RC Q_A in bRC reaction center			
	PhyQ or 2-Me-1,4-NQ quinone cofactor		2-phytyl-1,4-NQ quinone cofactor	2-ethyl-1,4-NQ quinone cofactor	UQ-10 quinone cofactor		$UQ_{10}^{-\bullet}$ in frozen solution	$PhyQ^{-\bullet}$ in frozen solution
	$A_1^{-\bullet}$ state		$P_{700}^{+\bullet}A_1^{-\bullet}$ state		$Q_A^{-\bullet}$ state			
	$-CH_3$ [a] residue	-CH_3 [b] residue	$-H$ [c] residue	$-CH_2-$ [d] residue	$-CH_3$ [e] residue	$-CH_3$ [f] residue	$-CH_3$ [g] residue	$-CH_3$ [a] residue
$A_{x'}$ ($A_\perp$)	9.1	8.8	−15.5	12.2	3.6	3.09	4.8	6.3
$A_{y'}$ ($A_\perp$)	9.1	8.8	−11.8	12.2	3.6	3.59	4.8	6.3
$A_{z'}$ ($A_\parallel$)	12.8	12.3	<|−5|	16.8	6.8	6.62	8.5	9.5
a_{iso}	10.3	10.0	≈−10.3	13.7	4.6	4.45	6.0	7.4
ρ^h	0.16	0.14	0.16	0.14	0.070		0.093	0.114

[a] Reference 11. [b] Reference 12. [c] Reference 25. [d] Reference 9. [e] Reference 7, bRC in frozen solution. [f] Reference 7, bRC in single crystal [g] Reference 27. [h] The spin density ρ represents the π-spin density at the ring carbon position 2 with the different substituents listed in line 4. It is calculated according to the appropriate McConnell equation.[17] For the α proton of an aromatic C−H group $a_{iso} = \rho_c^{(\pi)}Q$, with $Q_{CH} = -64.8$ MHz is used. For the methyl and ethyl groups a modified McConnell equation applies: $a_{iso} = \rho_c^{(\pi)}(B_0 + B_2\cos^2\theta)$ ($B_0 = 9$ MHz, $B_2 = 122$ MHz, θ dihedral angle between the plane of the C−C and C−H bonds and the axis of the p_z orbital). $\theta = 45°$ applies for the methyl group with free rotation about the C−CH_3 bond and $\theta = 30°$ for the $-CH_2-$ group, consistent with experimental results.[9]

Prior to the TR ESR measurements, 10 μL of 1 M ascorbate solution was added and the sample was dark-adapted and frozen in the dark.

Transient EPR Spectroscopy. X-band transient EPR experiments were carried out using a Bruker ER046 XK-T microwave bridge equipped with a Flexline dielectric resonator[16] and an Oxford liquid helium gas-flow cryostat. The loaded Q value for this dielectric ring resonator was about $Q = 3000$, equivalent to a rise time of $\tau_r = Q/(2\pi^*\nu_{mw}) \approx 50$ ns. Q-band (35 GHz) transient EPR spectra of the samples were also measured with the same setup except that a Bruker ER 056 QMV microwave bridge equipped with a home-built cylindrical resonator was used. The samples were illuminated using a Spectra Physics Nd:YAG/MOPO laser system operating at 10 Hz at either the second harmonic (532 nm) or near the long wavelength absorption edge of PS I at approximately 700 nm.

Results

Influence of the Hydrogen Bond on the Spin Density Distribution over the Quinone Ring. The general valence bond model for the asymmetric spin density distribution in a semiquinone radical anion (as reviewed[7]) is adapted in Figure 2 to the case of the 2-methyl-1,4-naphthoquinone radical anion with a single H-bond as in the Q_K−A site of PS I Figure 1 (bottom). According to this model, the partial positive charge, associated with a dominant (or single) H-bond to one quinone carbonyl group (for instance O_4 in the C═O group to which the phytyl tail is in a meta-position in Figure 1), increases the negative charge at this (O_4) oxygen atom at the cost of the charge in the ring as well as at O_1. In agreement with the possible resonance structures (see Figure 2), the spin density will shift to higher values at the position C_4, next to O_4, and at the alternating positions C_2, C_6, and O_1. At the odd ring positions between, a shift of the spin density to lower values is expected. A suitable reference would be the case of symmetric H-bonding associated with a symmetric spin density distribution as encountered in solution. However, the average spin density for the symmetry related ring positions will be higher in protic (e.g., 2-propanol) vs aprotic (1,2-dimethoxyethane/2-methyltetrahydrofuran) solvents. This model establishes a simple correlation between the asymmetry in H-bonding with the observed asymmetry in the spin density distribution. The spin densities, in turn, are evaluated from the EPR detected hyperfine tensor parameters. Normally, the McConnell relation $a_{iso} = Q\rho^\tau$ is used to evaluate the π-spin density at a ring position from the isotropic hfs constant measured for a nuclear spin to this ring position in substituent attached, such as the proton spin in a $-H$, $-CH_3$, or $-CH_2-$ fragment.[17] Due to the restricted motion in photosynthetic reaction centers, the full hfs tensor can be determined and a_{iso} can be evaluated from the tensor trace 1/3Tr(A) and compared with the value of a_{iso} for the radical ion in liquid solution. If quinones with the same local ring conformation (but, e.g., different H-bonding schemes) are compared in different RCs, the local electronic structure and the overall features of the hyperfine tensor like anisotropy, symmetry, etc. will remain unchanged. Under these conditions, the change in the most accurate measurable hfs tensor component can be directly related to the differences in spin density and H-bond arrangement between the compared binding sites.

The most detailed experimental data have been reported for the ubiquinone-10 radical anion in the Q_A site of *Rhodobacter sphaeroides*, for review see.[7,10] The hfs tensors of the methyl group and the first methylene protons of the isoprenyl chain in adjacent ring positions (see Figure 1) reveal opposite shifts of the respective spin densities (relative to the symmetric H-bonding case in isotropic solution)—in fact, a decreased spin density at the former ring position and a increased spin density at the latter ring position (see Table 1 for a summary of all data). In addition, with selective ^{13}C-labeling, the ring positions 1 to 4 have been addressed individually.[18−22] The evaluated spin densities reflect well the alternating shifts in the spin density distribution (Table 2) in the case of asymmetric H-bonding. In addition, each of the carbonyl groups has been labeled with ^{17}O and the π-spin densities in positions 1 and 4 were determined (as summarized in Table 2 of ref 7). Although the asymmetric shifts of the spin densities show considerable experimental scatter over the comparable various ring positions, the asymmetric H-bond pattern with a predominant H-bond to the O_4 carbonyl oxygen in the Q_A site of bRC (see Figure 1, top) is proven consistently.

For the type I RC in PS I, evidence for a high degree of asymmetry in H-bonding comes so far from the large hfs tensor elements measured for protons in just one ring position corresponding to that of the phylloquinone methyl group. Slightly different hfs tensor values have been determined for the stable photoaccumulated $Q_K^{-\bullet}$ anion[11] and the transient radical pair state.[12] The corresponding shift of the spin density is at least twice that for the methyl group in Q_A of the bRC and

TABLE 2: ^{13}C Hyperfine (hfs) Tensor Values (MHz) for Quinone Anions in Different Protein−Cofactor Systems

^{13}C-labeled quinone (site)	protein cofactor system	relative ring position: C−O group (with strong H-bond) to phytyl or isoprenyl chain	^{13}C hfs tensor principal values[a] A_{xx} A_{yy} A_{zz} for the ^{13}C−O group with high spin dens	low spin dens	sym av $\langle A_{zz}\rangle$	A_{zz} asym ΔA_{zz}
2-CH_3−1,4-NQ[b] (Q_K)	PS I	ortho	−10.5(15)			
			−10.5(15)	n.d.		
			+44.0(20)		{**30**}	{**28**}
UQ-10 (Q_A)[c]	ZnbRC	meta	−|< 7.0|(15)	−15.4(15)		
			−|< 7.0|(15)	−14.6(15)		
			+ **35.5**(8)	**22.4** (8)	**29.0**	**13.1**
UQ-3 (Q_A)[d]	ZnbRC	meta	−9.2(15)	−12.6(15)		
			−9.8(15)	−14.6(15)		
			+**35.0**(5)	**22.7** (5)	**28.9**	**12.3**
UQ-2(Q_H)[e]	ubiquinol oxidase cyt bo_3	ortho	−4.2(15)	−7.0(15)		
			−12.6(15)	−10.4(15)		
			+**30.8**(8)	**20.2**(8)	**25.5**	**10.6**

[a] Errors of hfs tensor values are given in parentheses with respect to the last digit. Signs of hfs tensor values are not determined in this study but are set as given in refs 19, 20, 26. [b] Preliminary ^{13}C hyperfine (hfs) tensor values determined from Q-band spectra (see Figure in Supporting Information) of reduced for 2-methyl-4-^{13}C-1,4-naphthoquinone in frozen 2-propanol-d_8 solution: $|A_{xx}| = 10$ MHz, $|A_{yy}| = 10$ MHz, and $|A_{zz}| = 30$ MHz (error ± 2 MHz). [c] Reference 19. [d] Reference 20. [e] Reference 26.

has the opposite sign. The latter is consistent with the fact that the methyl group is meta to the H-bonded carbonyl group of Q_K in PS I while for Q_A in bRC it is ortho to the carbonyl group with the dominant H-bond; see Figure 1. The increased spin density shift for PS I is consistent with the structural properties of only a single H-bond for Q_K in PS I.[1] The considerable significance and stability of such a special, highly asymmetric H-bonding for Q_K in PS I make it mandatory to check out the asymmetric spin density distribution for other ring positions. As demonstrated for the bRC, ^{13}C-labeled quinones offer reliable results. The most important ring position to test is the carbon nucleus of the H-bonded carbonyl group.

Efficiency of Quinone Replacement. For the preparation of PS I complexes with artificial quinones in the Q_K site, three different strategies have been introduced so far and proved to yield equivalent results[8,9] with respect to TR-EPR spectroscopy of the functional charge-separated state $P_{700}^{+\bullet}Q_K^{-\bullet}$: (1) reconstitution of artificial quinones in PS I complexes after extraction of the native phylloquinone with organic solvent; (2) use of mutant cells in which the phylloquinone biosynthetic pathway has been interrupted (e.g., *menB*[3,4]) and in which plastoquinone (PQ-9) has been recruited into the Q_K site and the artificial quinone is supplemented in vivo to the growth-media; (3) in vitro biochemical exchange of PQ-9 in PS I complexes isolated from the *menB* mutant. In this work, procedure 3 was used; PQ-9 recruited during cell growth into the Q_K site of PS I trimers isolated from *menB* mutant cells can be replaced with differently ^{13}C-labeled 2-methyl-1,4-naphthoquinones (see Figure 3). Substitution was checked to be complete, to the extent that the broader spectrum of the PQ-9 containing *menB* sample[4] cannot be observed to contribute to the spectra (see Figure 4) withing experimental accuracy of about 5%. The lower affinity of PQ-9 in the *menB* mutants compared to phylloquinone in the wild-type allows efficient incorporation of the nonnative quinone which is not possible with phylloquinone in the Q_K site.

In addition, 2-methyl-1,4-naphthoquinone has been shown to enter the Q_K site in the same position and orientation as phylloquinone in wild-type PS I complexes,[8,9] again within experimental accuracy. This is not expected to change and is confirmed here for both isotopically labeled 2-methyl-1,4-naphthoquinones.

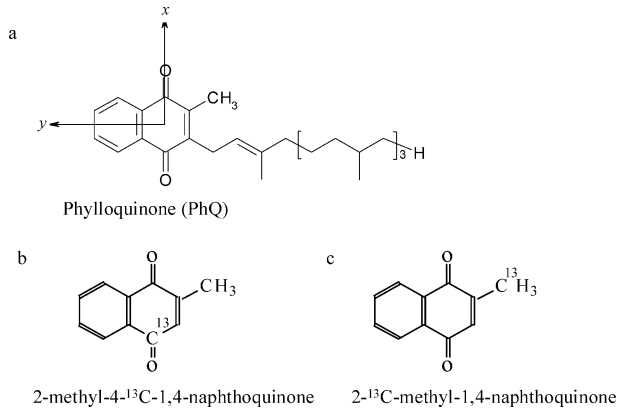

Figure 3. (a) Molecular structure of phylloquinone (vitamin K_1, 2-methyl-3-phytyl-1,4-naphthoquinone). The molecular axes shown also coincide with the **g** tensor principal axes of the quinone anion. (b) Molecular structure of 2-methyl-4-^{13}C-1,4-naphthoquinone. (c) Molecular structure of 2-^{13}C-methyl-1,4-naphthoquinone. The molecules shown in parts b and c have been used for incorporation into the A_1 site in PS I.

TR-EPR Results. Figure 4 presents the X-band (top) and Q-band (bottom) spin polarized spectra of the transient radical pair state $P_{700}^{+\bullet}NQ^{-\bullet}$ for PS I samples with the following set of naphthoquinones in the A_1 site: native phylloquinone, 2-methyl-1,4-naphthoquinone, 2-methyl-4-^{13}C-1,4-naphthoquinone, and 2-^{13}C-methyl-1,4-naphthoquinone. Except for the different (partially resolved) hyperfine splittings, all the transient spectra exhibit the same overall polarization pattern as for native phylloquinone in PS I, i.e., E/A/E (E = emission, A = absorption) at X-band and E/A/A/E/A at Q-band. In conjunction with the well-understood (high field/high frequency) spectra in wild-type PS I,[5,6] this confirms that the artificial quinones take up the same position and orientation as native phylloquinone in wild type, at least within the error limits discussed in refs 5 and 6. In contrast, the spectral patterns in Figure 4 differ significantly with respect to the partially resolved hyperfine multiplets. For native PS I, a well-understood quartet is observed[6] with relative intensities of 1:3:3:1 centered at a g_{eff} spectral position near the g_{yy} component of the quinone **g** tensor. This hfs multiplet corresponds fully to the nearly axially symmetric methyl hfs tensor with slightly different principal

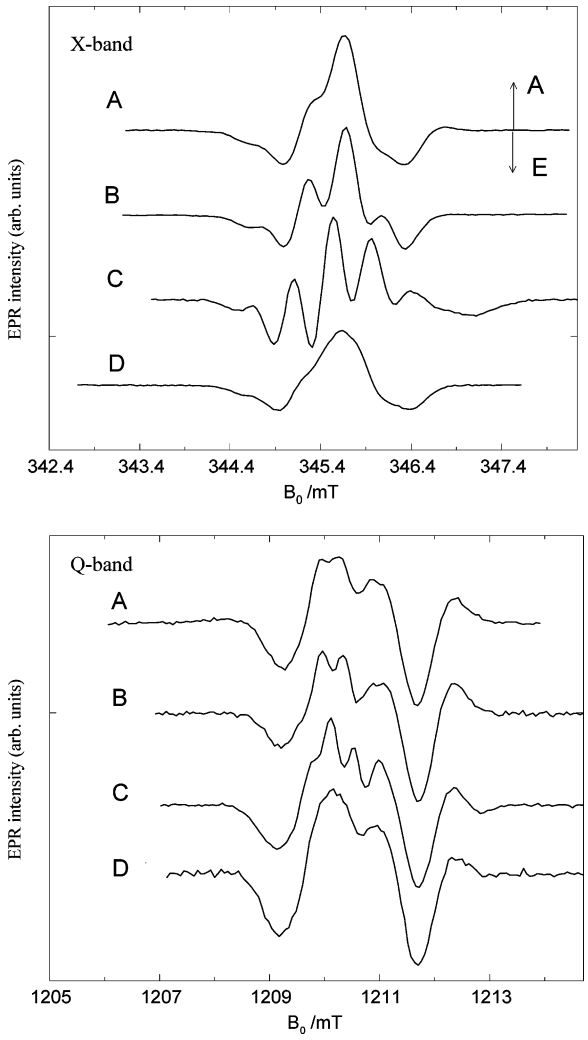

Figure 4. Spin polarized transient EPR spectra of the $P_{700}^{+\bullet}NQ^{-\bullet}$ radical pair state in PS I particles at 80 K. Comparison of spectra with native phylloquinone (A), 2-methyl-1,4-naphthoquinone (B), 2-methyl-4-^{13}C-1,4-naphthoquinone (C), and 2-^{13}C-methyl-1,4-naphthoquinone (D) in the A_1 binding site of the *menB* mutant (for molecular structures see Figure 3). Top: X-band. Bottom: Q-band.

values (see Table 1) as determined by cw-ENDOR[11] for the photoaccumulated $A_1^{-\bullet}$ anion or by pulsed ENDOR[12] for the transient $P_{700}^{+\bullet}A_1^{-\bullet}$ state. The 1:3:3:1 hfs multiplet is even better resolved for 2-methyl-1,4-naphthoquinone (**V**K_3) (Figure 4, second spectrum from top). Indeed, the remaining inhomogeneous line width is reduced due to the smaller number of nearby proton spins when the phytyl side chain is absent.

In Figure 4 (bottom spectrum) the same methyl hyperfine splitting is broadened beyond resolution for 2-^{13}C-methyl-1,4-naphthoquinone both at X- and Q-band due to the additional hfs of the ^{13}C nuclear spin in the methyl group. However, the methyl proton hyperfine tensor remained unchanged as confirmed by pulsed ENDOR spectroscopy for 2-methyl-1,4-naphthoquinone and native phylloquinone (data not shown). As noted previously in solution and in bRC studies of benzoquinones, ENDOR lines due to ^{13}C hfs could not be observed.[22]

The X-band spectrum of the $P_{700}^{+\bullet}NQ^{-\bullet}$ radical pair state with 2-methyl-4-^{13}C-1,4-naphthoquinone in the A_1 site shows the most significant differences. Correlated changes can be seen in the Q-band spectra of Figure 4 bottom: (1) The overall spectral width is clearly wider. (2) The partially resolved hyperfine pattern becomes more complex due to the additional ^{13}C hyperfine splitting. (3) A direct indication of a very large (out-of-plane) A_{zz} component of the ^{13}C hyperfine tensor is the additional broad emissive spectral component at the high field end of both the X- and Q-band spectra. This component is specific to the spin polarization pattern of this sample only. Corresponding spectral effects have been observed in cw Q-band spectra of the bRC reconstituted with isotope-labeled ubiquinones[18,19,21] and assigned to the hyperfine tensor elements of the ^{13}C label in the carbonyl group to which the dominant H-bond is attached. However, already a qualitative comparison indicates that the ^{13}C hyperfine tensor elements are substantially larger for the quinone in PS I vs the bRC.

^{13}C Hyperfine Tensor Parameters from Spectra Simulations. To achieve a more quantitative evaluation of the ^{13}C hfs tensor elements, simulations of the transient spectra were carried out. The correlated radical pair (CRP) concept is well established and extensively tested for the native $P_{700}^{+\bullet}A_1^{-\bullet}$ multifrequency spectra.[5,6,23] A large number of magnetic interaction and structural parameters are needed for spectra simulation. Most are known from independent experimental data. Convincing spectral simulations have been achieved for the $P_{700}^{+\bullet}A_1^{-\bullet}$ state of wild-type PS I.[6] All these magnetic interaction parameters and relative tensor orientations are listed in a table in the Supporting Information and are used for the present simulations with a slight adjustment of quinone **g** tensor parameters.[9] Indistinguishable relative orientations between the **g** tensors of quinone and P_{700} have been mentioned previously for 2-methyl-1,4-naphthoquinone and native phylloquinone in the A_1 site. This was checked most reliably for fully deuterated 2-methyl-1,4-naphthoquinone.[9] The partially resolved largest hyperfine splitting due to the hfs tensors of the methyl protons and the ^{13}C spin have been considered explicitly as the only adjustable parameters in the present simulations. Note that all other parameters including those related to structure and relative orientations have been kept unchanged for all isotopically labeled 2-methyl-1,4-naphthoquinones. In conclusion, for the simulation all parameters stay fixed with the exception of the two parameters needed for the nearly axially symmetric ^{13}C-hfs tensor. The principal axis orientations of the ^{13}C-hf tensors coincide with those of the quinone molecular plane. The *z*-axis is collinear with the out-of-plane axis. The largest ^{13}C hyperfine splitting is expected along this axis. It will be most clearly resolved in the EPR spectra as demonstrated previously with ^{13}C-labeled quinones in the bRC.

In Figure 5, X- and Q-band TR-EPR powder spectra are simulated for 2-methyl-4-^{13}C-1,4-naphthoquinone in the A_1 site. The hyperfine coupling constant A_{zz}(^{13}C) was varied between 36 and 48 MHz (in steps of 4 MHz). This parameter appears to be most sensitive to the shift of the emissive high field component in the spectra. The best agreement with the experimental spectra is achieved for $A_{zz} = 44$ MHz with an error of ± 2 MHz. The additional hfs multiplet splitting observed in the lower field region of the X-band spectra allows the A_{xx} and A_{yy} hfs values to be deteremined in the 9−12 MHz range. These ^{13}C-hfs tensor values are included in Table 2, which compares the combined data for the bRC and for PS I. While the spectral position of the partially resolved hyperfine splitting are simulated very well, the relative intensities are not. This is usually fixed by additional anisotropic line width parameters.[32] Here, only a single line width parameter was used for $P_{700}^{+\bullet}$ and $NQ^{-\bullet}$ to emphasize the spectral effect of the hfs coupling constants only.

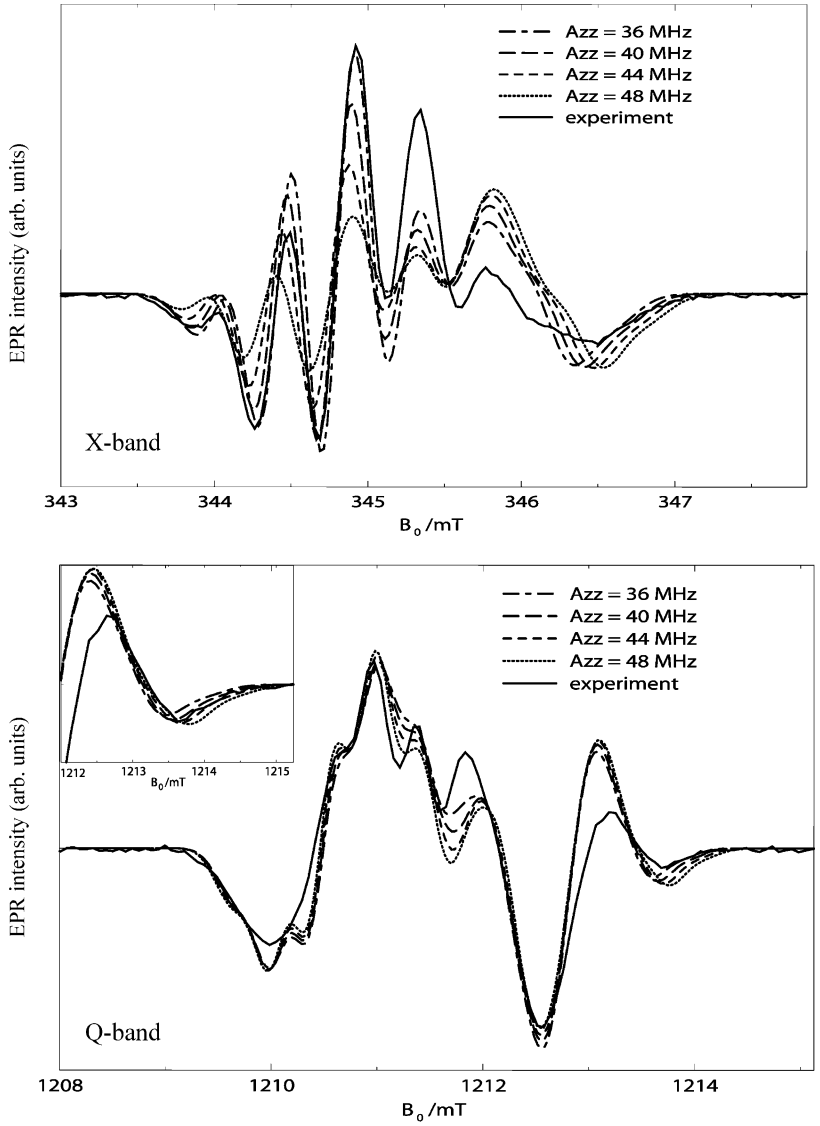

Figure 5. Comparison of experimental spin polarized transient EPR spectra of the $P_{700}^{+\bullet}NQ^{-\bullet}$ radical pair state in PS I particles with 2-methyl-4-^{13}C-1,4-naphthoquinone in the A_1 binding site (as in Figure 4) with simulated spectra according to the spin correlated radical pair model. The structural and magnetic tensor parameters used for the simulation are collected in the table in Supporting Information. Only the A_{zz} value was varied as indicated. Top: X-band. Bottom: Q-band.

Discussion

This study extends the determination of the asymmetric spin density distribution to another significant ring position of the quinone in the functional $P_{700}^{+\bullet}$ $A_1^{-\bullet}$ state of PS I. The principal spectroscopic indicator for the highly asymmetric and alternating spin density distribution of the $A_1^{-\bullet}$ radical ion was thus far the unusually large upshift toward an increased spin density at the ring position of the methyl group of native phylloquinone in PS I. The degree of asymmetry is interpreted to directly reflect the asymmetry of the H-bonding to the two carbonyl groups of the quinone as demonstrated before in the case of bacterial reaction centers, see ref 7 for a review. All relevant proton hyperfine tensor components and spin densities evaluated for the respective ring position have been collected in Table 1 and compared with corresponding data in bRC. In PS I essentially the same increased spin density (0.14−0.16) is evaluated from the hyperfine tensor components measured for such different substituents as the native methyl group (first two columns of Table 1) or the aromatic C−H fragment (third column) as obtained for 2-phytyl-1,4-naphthoquinone in the A_1 site of PS I from the *men*G mutant of *Synechococcus* sp. PCC 7002.[25] More surprising and not fully explained yet is the observation that a single substituent in the form of an *n*-alkyl chain (or $-(CH_2)_{n-1}-CH_3$) is incorporated into the A_1 site, occupying the position of the methyl group and not as expected that of the phytyl chain as in native phylloquinone.[9] The hyperfine tensor elements measured for the first methylene group are also listed in Table 1 (fourth column) and turn out to be in quantitative agreement with the same increased spin density in this ring position.[9] In addition, the observed a_{iso} value requires a certain conformation of the alkyl substituent with the dihedral angle $\theta = 30°$ between the plane of the C−C and C−H bonds and the axis of the p_z orbital.

For comparison Table 1 includes hyperfine parameters for the Q_A site of bRC in frozen solution and in single crystals (columns 4 and 5) and for the respective quinone anions in frozen isotropic solution (last two columns). For this comparison, the CH_3 group of the quinone acceptor in the Q_A site of bRC was chosen. Because the dominant H-bond is attached to opposite carbonyl groups (with respect to the same ring position for the phytyl/isoprenyl chain, see Figure 1), the a_{iso} value of about 6.1 MHz ($UQ^{-\bullet}$) and 7.4 MHz ($PhyQ^{-\bullet}$) in the symmetric

H-bond situation in isotropic solution are shifted in opposite direction, i.e. down to about 4.5 MHz in the bRC but up to about 10 MHz in PS I (see Table 1). Correspondingly, the spin density shifts from a solution value down by $\Delta\rho \approx 0.023$ for Q_A in bRC but up $\Delta\rho \approx 0.036$ for Q_K. The ratio of these shifts yields $|\Delta\rho(Q_K)/\Delta\rho(Q_A)| \approx 1.6$ and is on average independent of the substituent chosen in place of the $-CH_3$ group of the quinone acceptor in PS I. In connection with the significance of these spin density shifts and their correlation with a larger asymmetry of H-bonding in PS I it seemed mandatory to extent these studies to at least one other significant ring position as achieved here by selective ^{13}C isotope labeling of the naphthoquinone cofactor.

Table 2 collects the relevant ^{13}C hyperfine tensor elements determined for the two possible ring positions associated with the quinone carbonyl groups for different protein−quinone cofactor systems. In the asymmetric environment within the protein, one of the quinone C═O groups will have a stronger H-bond and the corresponding carbon position is termed high spin density; the other C═O group with a weaker or no H-bond is termed low spin density. For the ^{13}C hfs tensor of a ring carbon position the a_{iso} value is usually small, and the analogue of a McConnell relation is difficult to apply (for details, see ref 7). Therefore, a different strategy than for the protons is followed for the analysis of the asymmetry in the spin density distribution.

In Table 2, complete sets of ^{13}C hfs tensor elements are listed for each of the ^{13}C-labeled carbonyl groups of different ubiquinones in the Q_A site of purple bacterial reaction centers as determined by two laboratories[18,19] and[20,21] and recently in the Q_H site of ubiquinol oxidase cyt bo_3.[26] Comparison of the various ^{13}C hyperfine tensor elements reveals clear general characteristics. All ^{13}C hyperfine tensors listed are highly anisotropic with nearly cylindric symmetry. The largest component A_{zz} along the out-of-plane axis and the nearly equal in-plane components have opposite signs. This corresponds to a common structure of the ^{13}C hfs tensor for all quinone carbonyl groups involved as expected for a highly local property. On the other hand, the different environments and correspondingly different protein cofactor interactions are known to influence strongly the general quinone electronic structure and with it features like spin density distribution and **g** tensors but, as we saw, not the structure of the ^{13}C hfs tensor. The consequence of the latter empirically tested fact is that the largest and most accurately measurable hfs tensor component A_{zz} will directly reflect relative changes in spin density and H-bond asymmetry.

To determine the asymmetry between the two carbonyl hyperfine tensors two strategies have been followed: (a) Measurement of the ^{13}C-labeled and unlabeled $Q^{-\bullet}$ radical anions in liquid and frozen isotropic solution. Symmetric H-bonds are assumed and thus averaged hfs tensor elements are obtained. (b) Each of the carbonyl groups is labeled selectively. The asymmetry is measured directly and the mean value can be evaluated. Both methods have been applied for $UQ^{-\bullet}$ in bRC and bo_3 and provided consistent results within a sufficient error margin. The comparison of just the A_{zz} values also yields consistent results. A_{zz} values measured for a series of ^{13}C-labeled ubiquinones in frozen solution[19,20,22] compare on average well with the average $\langle A_{zz}\rangle$ values listed in Table 2 for the different Q sites in the different protein systems.

On the basis of the following arguments, the average $\langle A_{zz}\rangle$ value of about 29 MHz ($UQ^{-\bullet}$ in bRC) can be taken over for $NQ^{-\bullet}$ in PS I. The main spin density is located on the two carbonyl groups and the spin density moved into the second ring of NQ is neglible as confirmed by spin density calculations as well as experiments. Therefore, independent of very different asymmetries between the two carbonyl groups the average $\langle A_{zz}\rangle$ value will be about the same. This can be tested by measuring the average $\langle A_{zz}\rangle$ value for the ^{13}C-labeled $NQ^{-\bullet}$ in isotropic solution. A value $\langle A_{zz}\rangle$ of 30 ± 2 MHz (Table 2, footnote *b*) is evaluated from Q-band spectra (figure in Supporting Information). Method b has not been applied yet, and specific difficulties are anticipated. Because of the large asymmetry for $NQ^{-\bullet}$ in PS I, the ^{13}C hyperfine values for the low spin density carbonyl group are expected to be difficult to measure accurately and may require more elaborate techniques. Second, the ^{13}C hyperfine structure tensor may be distorted significantly due to increased spin densities in the neighboring ring positions. Because of these difficulties, we have opted to put the ^{13}C label only in ring positions with high spin density.

As documented with Table 2 all ^{13}C hyperfine parameters are considerably increased in PS I, in particular the asymmetry parameter ΔA_{zz} is more than double of the bRC and bo_3 values. The ratio $|\Delta A_{zz}(Q_K \text{ in PS I})/\Delta A_{zz}(Q_A \text{ in bRC})| \approx 2.1$ can be compared with the ratio $|\Delta\rho(Q_K)/\Delta\rho(Q_A)| \approx 1.6$ as determined above from proton hfs couplings at the ring position of the methyl group in native phylloquinone. Given the respective error margins and approximations made, these values agree very well. Comparably large asymmetry demonstrated for the two most significant ring positions confirms nicely the valence bond model as illustrated in Figure 2. The correlation between the measured hyperfine or spin density parameters and the large asymmetry of the H-bonds for the functional $P_{700}^{+\bullet}$ $A_1^{-\bullet}$ state of PS I has been established much better.

The highest asymmetry in spin density distribution and H-bonding for the quinone in the $A_1(Q_K)$ site of PS I is consistent with the H-bond schemes suggested by the respective X-ray structure models. As shown with the comparison in Figure 1, only a single backbone H-bond is anticipated for the Q_K site in PS I in contrast to two asymmetric H-bonds for the Q_A site in the bRC. Even more than two H-bonds are expected from the structural model of the Q_H site in cyt bo_3 (see Figure 1B of ref 26). In that respect, the one dominant H-bond for the A_1 site of PS I (as opposed to multiple, compensating H-bonds in the other systems) is a straightforward explanation for the observed increased asymmetry effects for the A_1 site in PS I. On the other hand, the structural comparison of the quinone binding sites in PS I and the bRC (Figure 1) shows that the one H-bond to the backbone involves in both cases the C═O group which is in ortho-position to the phytyl-/isoprenyl-chain substituent, respectively. However, the dominant H-bond for the Q_A site in the bRC concerns the other C═O group with the H-bond to the histidine residue that also provides a ligand to the non-heme iron. As a result, the asymmetry effects have the opposite sign for the Q_A site in bRC as compared to the other systems in Table 2. In other words, either the H-bond to the histidine is sufficiently strong to overcompensate the second backbone H-bond for the Q_A site in the bRC or the latter is relatively weak. Close inspection of the X-ray structures does not provide an obvious structural indication that the single backbone H-bond for the A_1 site of PS I is stronger than the backbone H-bond for the Q_A site in bRC. The main structural indicators such as length and angles for the quinone hydrogen bonds to the respective −NH− backbone group exhibit only minor differences for the bRC and PS I. Despite this, the considerably larger asymmetry effects observed for the functionally relevant A_1 site in PS I are explained most readily by a correspondingly stronger backbone H-bond in PS I than in bRC. A further hint comes from the fact that this backbone

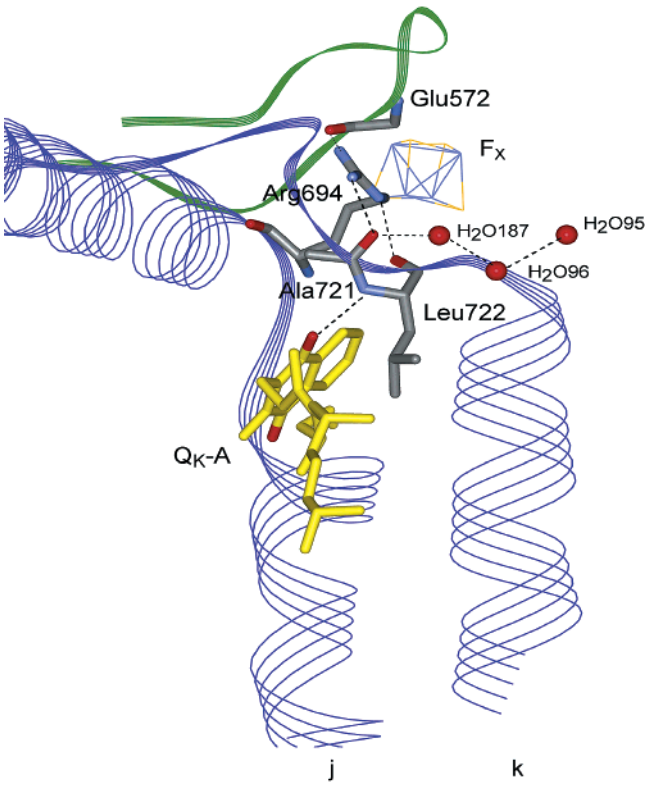

Figure 6. Hydrogen bond network in the neighborhood of the Q_K-A site and the characteristic H-bond with the backbone of $Leu722_{PsaA}$. The $Arg694_{PsaA}$ residue at the start of the stromal surface helix **jk**(1) bridges the j−k return loop (including the neighbors $Ala721_{PsaA}$ and $Leu722_{PsaA}$) and $Glu572_{PsaB}$ of the F_X binding loop provided from PsaB. It also connects to a set of water molecules H-bonded among each other.

H-bond in PS I is highly stable. As seen with the examples in Table 1, the asymmetry effects remain essentially unaffected even if substantial changes occur in the size and molecular structure of the substituents in either the place of the methyl group or the phytyl chain of native phylloquinone. Strength and stability of the particular backbone H-bond between the quinone appear to be characteristic features of the A_1 site in PS I.

Cooperative effects due to hydrogen bond networks that may involve a more distant protein environment have been suggested as a mechanism for increased backbone H-bond strength.[28] Indeed, an extended H-bond network can be identified in the PS I structure surrounding the Q_K site part of which is shown in Figure 6 for the Q_K-A site. At the center is the $Arg694_{PsaA}$ residue, located at the start of the stromal surface helix **jk**(1). It acts as a bridge with H-bonds to the j−k return loop of PsaA (including $Ala721_{PsaA}$, $Leu722_{PsaA}$) on one side and on the other side to the F_X binding loop provided by the h−i loop of PsaB via an intersubunit H-bond between the NH(1) group of $R694_{PsaA}$ and the backbone oxygen of $G572_{PsaB}$; see ref 29 for more details. The H-bonds described are part of an extended network that could also function as a possible electron-transfer pathway between A_0 via quinone to F_X. Initial experimental results with a mutation of the $Arg694_{PsaA}$ residue have been described in ref 13. Figure 6 shows that the H-bond network extends even further, from the backbone oxygen of $Ala721_{PsaA}$ to a set of water molecules hydrogen bonded among each other. It is suggested that the whole H-bond network adds to the stability and strength of the one backbone H-bond to the quinone. Note that for the C_2 symmetry related Q_K-B site similar features exist as shown in Figure 6 for the Q_K-A site.

The confirmation provided in this work for a highly asymmetric, fairly strong and highly stable hydrogen bond between the quinone cofactor and the protein backbone suggests to intensify the search for evidence of this H-bond and its proton hfs tensor with pulsed ENDOR techniques. Recent work on the photoaccumulated $A_1^{-\bullet}$ radical anion in frozen solution is contradictory because it concludes the existence of two H-bonds per quinone.[30] In contrast, pulsed ENDOR spectroscopy of the A_1^- state in PS I single crystals indicates only one H-bond hyperfine tensor per quinone[31] as suggested by the structure. Ongoing ENDOR studies of H-bonds both in isotropic polar solution[32] and for the quinone binding sites in bRC[33] and in PS I[34] are expected to provide more detailed insight into understand the particular strength of the quinone backbone H-bond in PS I as well.

Acknowledgment. The authors would like to acknowledge Christian Teutloff for assistance with the pulsed ENDOR experiments, W. Lubitz for providing access to the pulsed ENDOR instrument and Gaozhong Shen for isolating PS I complexes from the *menB* mutant of *Synechocystis* sp. PCC 6803. Funding was provided by the Deutsche Forschungsgemeinschaft (Sfb 498, A3) and National Science Foundation (MCB-1107079 to J.H.G.).

Supporting Information Available: A table containg **g** tensor and other magnetic interaction as well as structural parameters as obtained from independent experimental data and used for the simulation of transient EPR spectra of the $P_{700}^{+\bullet} + Q^{-\bullet}$ state in this paper and a figure showing the Q-band EPR spectrum of 2-methyl-4-^{13}C-1,4-naphthoquinone anion radical in 2-propanol-d_8. This material is available free of charge via the Internet at http://pubs.acs.org.

References and Notes

(1) Jordan, P.; Fromme, P.; Witt, H. T.; Klukas, O.; Saenger, W.; Krauss, N. *Nature (London)* **2001**, *411*, 909−917.
(2) Fromme, P.; Jordan, P.; Krauss, N. *Biochim. Biophys. Acta* **2001**, *1507*, 5−31.
(3) Johnson, T. W.; Shen, G.; Zybailov, B.; Kolling, D.; Reategui, R.; Beauparlant, S.; Vassiliev, I. R.; Bryant, D. A.; Jones, A. D.; Golbeck, J. H.; Chitnis, P. R. *J. Biol. Chem.* **2000**, *275*, 8523−8530.
(4) Zybailov, B.; van der Est, Art; Zech, S. G.; Teutloff, C.; Johnson, T. W.; Shen, G.; Bittl, R.; Stehlik, D.; Chitnis, P. R.; Golbeck, J. H. *J. Biol. Chem.* **2000**, *275*, 8531−8539.
(5) Kamlowski, A.; Zech, S.; Fromme, P.; Bittl, R.; Lubitz, W.; Witt, H. T.; Stehlik, D. *J. Phys. Chem. B* **1998**, *102*, 8266.
(6) Zech, S. G.; Hofbauer, W.; Kamlowski, A.; Fromme, P.; Stehlik, D.; Lubitz, W.; Bittl, R. *J. Phys. Chem.* **2000**, *104*, 9728−9739.
(7) Lubitz, W.; Feher, G. *Appl. Magn, Reson* **1999**, *17*, 1−48.
(8) Johnson, T. W.; Zybailov, B.; Jones, A. D.; Bittl, R.; Zech, S. G.; Stehlik, D.; Golbeck, J. H.; Chitnis, P. R. *J. Biol. Chem.* **2001**, *276*, 39512−39521.
(9) Pushkar, Y. N.; Zech, S. G.; Brown, S.; van der Est, A.; Zimmermann, H.; Stehlik, D. *J. Phys. Chem.* **2002**, *106*, 12052−12058.
(10) Hoff, A. J.; Deisenhofer, J. *Phys. Rep.* **1997**, *287*, 113−137.
(11) Rigby, S. E. J.; Evans, M. C. W.; Heathcote, P. *Biochemistry* **1996**, *35*, 6651−6656.
(12) Fursmann, C.; Teutloff, C.; Bittl, R. *J. Phys. Chem. B* **2002**, *106*, 9679−9686.
(13) Xu, Wu; Chitnis, P.; Valieva, A.; van der Est, A.; Pushkar, Y. N.; Krzystyniak, M.; Teutloff, C.; Zech, S. G.; Bittl, R.; Stehlik, D.; Zybailov, B.; Shen, G.; Golbeck, J. H. *J. Biol. Chem.* **2003**, *278*, 27864−27875.
(14) *Org. React*. **1942**, *I*, 251.
(15) Bhati, A.; Kale, N. *Angew. Chem.* **1967**, *79*, 1100.
(16) van der Est, A.; Hager-Braun, C.; Leibl, W.; Hauska, G.; Stehlik, D. *Biochim. Biophys. Acta* **1998**, *1409*, 87−98.
(17) Carrington, A.; McLachlan, A. *Introduction to magnetic resonance*; Harper and Row: New York, 1969; Chapter 7.
(18) Hoff, A. J.; Kropacheva, T. N.; Samoilova, R. I.; Gritzan, N. P.; Raap, J.; van der Brink, J. S.; Gast, U.; Lugtenburg, J. In *The Reaction Center of Photosynthetic Bacteria, Structure and Dynamics*; Michel-Beyerle, M.-E., Ed.; Springer: Berlin, 1996; pp 405−420.

(19) van der Brink, J. S.; Spoyalov, A. P.; Gast, P.; van Liemt, W.; Raap, J.; Lugtenburg, J.; Hoff, A. J. *FEBS Lett.* **1994**, *353*, 273−276.

(20) Feher, G.; Isaacson, R. A.; Okamura, M. Y.; Lubitz, W. In *Antennas and Reaction Centers of Photosynthetic Bacteria−Structure, Interactions and Dynamics*; Michel-Beyerle, M. E., Ed.; Springer Series in Chemical Physics; Springer: Berlin, 1985; Vol. 42, pp 174−189.

(21) Isaacson, R. A.; Abresch, E. C.; Lendzian, F.; Boullais, C.; Paddock, M. L.; Mioskowski, C.; Lubitz, W.; Feher, G. In: *The reaction center of photosynthetic bacteria, structure and dynamics*; Michel-Beyerle, M.-E., Ed.; Springer: Berlin, 1996; pp 353−367.

(22) Nimz, O.; Lendzian, F.; Boullais, C.; Lubitz, W. *Appl. Magn. Reson.* **1998**, 255−274.

(23) Prisner, T. F.; van der Est, A.; Bittl, R.; Lubitz, W.; Stehlik, D.; Moebius, K. *Chem. Phys.* **1995**, *195*, 361−370.

(24) Itoh, S.; Iwaki, M.; Ikegami, I. *Biochim. Biophys. Acta* **2001**, *1507* (1−3), 115−138.

(25) Sakuragi, Y.; Zybailov, B.; Shen, G.; Jones, A. D.; Chitnis, P. R.; van der Est, A.; Bittl, R.; Zech, S. G.; Stehlik, D.; Golbeck, J. H.; Bryant. D. A. *Biochemistry* **2002**, *41*, 394−405.

(26) Grimaldi, S.; Ostermann, T.; Weiden, N.; Mogi, T.; Miyoshi, H.; Ludwig, B.; Michel, H.; Prisner, T. F.; MacMillan, F. *Biochemistry* **2003**, *42*, 5632−5639.

(27) MacMillan, F.; Lendzian, F.; Lubitz, W. *Magn. Reson. Chem.* **1995**, *33*, 81.

(28) Jeffrey, G. A.; Saenger, W. *Hydrogen bonding in biological structures*; Springer-Verlag: Berlin, 1994.

(29) Antonkine, M.; Jordan, P.; Fromme, P.; Krauss, N.; Golbeck, J.; Stehlik, D. *J. Mol. Biol.* **2003**, *327*, 671−697.

(30) Purton, S.; Stevens, D. R.; Muhiuddin, I. P.; Evans, M. C.; Carter, S.; Rigby, S. E.; Heathcote, P. *Biochemistry* **2001**, *40*, 2167−2175.

(31) Teutloff, C. Ph.D. Thesis 2003 Technische Universität, Berlin.

(32) Flores, M.; Isaacson, R. A.; Calvo, R.; Feher, G.; Lubitz, W. *Chem. Phys.* **2003**, *294*, 401.

(33) Flores, M.; Isaacson, A.; Lubitz, W.; Feher, G. *Biophys. J.* **2003**, *84*, 120a.

(34) Pushkar, Y.; Stehlik, D.; van Gastel, M.; Lubitz, W. *J. Mol. Struct.* **2004**, in press.